NAVAL POSTGRADUATE SCHOOL
MONTEREY, CALIFORNIA

THESIS

OPTICAL CHARACTERISTICS OF LEXEL 85 ARGON ION LASER AND GSANGER LM0202P MODULATOR: APPLICATION TO AM-FM LIGHT CONVERSION

by

Harlan V. Wallace

June, 1996

Thesis Advisor: D. Scott Davis
Andres Larraza

Approved for public release; distribution is unlimited.

DISCLAIMER NOTICE

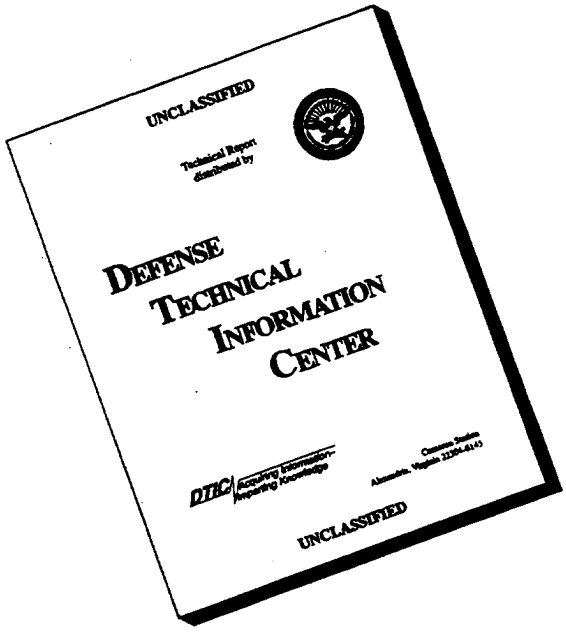

THIS DOCUMENT IS BEST QUALITY AVAILABLE. THE COPY FURNISHED TO DTIC CONTAINED A SIGNIFICANT NUMBER OF PAGES WHICH DO NOT REPRODUCE LEGIBLY.

REPORT DOCUMENTATION PAGE

Form Approved OMB No. 0704-0188

1. AGENCY USE ONLY *(Leave blank)*	2. REPORT DATE June, 1996	3. REPORT TYPE AND DATES COVERED Master's Thesis

4. TITLE AND SUBTITLE OPTICAL CHARACTERIZATION OF LEXEL 85 ARGON ION LASER AND GSANGER LM0202P MODULATOR: APPLICATION TO AM-FM LIGHT CONVERSION

5. FUNDING NUMBERS

6. AUTHOR(S) Harlan V. Wallace

7. PERFORMING ORGANIZATION NAME(S) AND ADDRESS(ES)
Naval Postgraduate School
Monterey CA 93943-5000

8. PERFORMING ORGANIZATION REPORT NUMBER

9. SPONSORING/MONITORING AGENCY NAME(S) AND ADDRESS(ES)

10. SPONSORING/MONITORING AGENCY REPORT NUMBER

11. SUPPLEMENTARY NOTES The views expressed in this thesis are those of the author and do not reflect the official policy or position of the Department of Defense or the U.S. Government.

12a. DISTRIBUTION/AVAILABILITY STATEMENT
Approved for public release; distribution is unlimited.

12b. DISTRIBUTION CODE

13. ABSTRACT *(maximum 200 words)*

The purpose of this thesis is to examine the possibility of using a commercial electro-optical modulator, the LM0202P modulator manufactured by Gsanger Opto-Elektronic of Germany, to amplitude modulate an argon ion laser, the LEXEL model 85, for proving a theory of the conversion of amplitude to frequency modulation of light in fiber optics. The main focus is to analyze the spectral output of the laser both before and after being directed through the modulator. Also to be considered is launching the laser light down a length of optical fiber. It was determined that the laser does not produce a single mode, monochromatic spectral line. Further, it was determined that when the laser is directed through the modulator, the structure on the laser profile tends to blur. This effect increases when DC bias voltage is applied to the modulator. Additionally, when the modulator is driven with an AC modulation superimposed on the DC bias voltage, the resultant optical spectral profile does not correspond to that expected for sinusoidal amplitude modulation.

14. SUBJECT TERMS Spectral Analyis of Argon Ion Laser

15. NUMBER OF PAGES 57

16. PRICE CODE

17. SECURITY CLASSIFICATION OF REPORT	18. SECURITY CLASSIFICATION OF THIS PAGE	19. SECURITY CLASSIFICATION OF ABSTRACT	20. LIMITATION OF ABSTRACT
Unclassified	Unclassified	Unclassified	UL

NSN 7540-01-280-5500

Standard Form 298 (Rev. 2-89)
Prescribed by ANSI Std. 239-18 298-102

Approved for public release; distribution is unlimited.

OPTICAL CHARACTERISTICS OF LEXEL 85 ARGON ION LASER AND GSANGER LM0202P MODULATOR: APPLICATION TO AM-FM LIGHT CONVERSION

Harlan V. Wallace
Lieutenant, United States Coast Guard
B.S., University of Utah, 1989

Submitted in partial fulfillment
of the requirements for the degree of

MASTER OF SCIENCE IN PHYSICS

from the

NAVAL POSTGRADUATE SCHOOL
June, 1996

Author: H V Wallace
Harlan V. Wallace

Approved by: D. Scott Davis
D. Scott Davis, Thesis Advisor

A. Larraza
Andres Larraza, Thesis Advisor

W. B. Colson
William Colson, Chairman
Department of Physics

ABSTRACT

The purpose of this thesis is to examine the possibility of using a commercial electro-optical modulator, the LM0202P modulator manufactured by Gsanger Opto-Elektronik of Germany, to amplitude modulate an argon ion laser, the LEXEL model 85, for proving a theory of the conversion of amplitude to frequency modulation of light in fiber optics. The main focus is to analyze the spectral output of the laser both before and after being directed through the modulator. Also to be considered is launching the laser light down a length of optical fiber. It was determined that the laser does not produce a single mode, monochromatic spectral line. Further, it was determined that when the laser is directed through the modulator, the structure on the laser profile tends to blur. This effect increases when DC bias voltage is applied to the modulator. Additionally, when the modulator is driven with an AC modulation superimposed on the DC bias voltage, the resultant optical spectral profile does not correspond to that expected for sinusoidal amplitude modulation.

TABLE OF CONTENTS

I. INTRODUCTION

Due to self-interaction effects, the frequency of a wave in a dispersive medium is amplitude dependent, and in the weakly nonlinear regime it is of the form

$$\omega(k) = \omega_0(k) + \omega_2(k)e \ . \qquad (1.1)$$

In expression (1.1), $\omega_0(k)$ is the linear dispersion relation, $\omega_2(k)$ is the nonlinear coefficient, and e is the energy density which is proportional to the square of the wave amplitude. For the case of fixed frequency, positive group velocity, and $\omega_2 > 0$, the effect of nonlinearity is to decrease the wavenumber k as the amplitude of the wave field increases.

To understand the combined effects of dispersion and nonlinearity, we follow closely the physical argument given by Larraza and Coleman [1]. Consider an initial state of a modulated wave observed in a frame moving with the group velocity (Figure 1a). An observer in this frame would see the crests of the wave propagate. Because of dispersion, the group and phase velocities are different.

Consider now the case where the nonlinear coefficient $\omega_2>0$. An observer in the frame moving with the linear group velocity would observe bunching of the crests when the modulation amplitude is low and anti-bunching when the modulation amplitude is high (Figure 1b). For positive dispersion, $\omega''(k)>0$,

$$\delta v_g = \omega''(k)\delta k \qquad (1.2)$$

increases towards the troughs of the modulation. Dispersive effects cause the energy to approach the troughs of the envelope, and the modulation propagates. Thus, to an observer moving with the linear group velocity, the modulation is no longer stationary. Instead, the modulation can propagate with both a velocity that is either higher or lower than the linear group velocity. This result is general, when the product $\omega_2\omega''$ is positive.

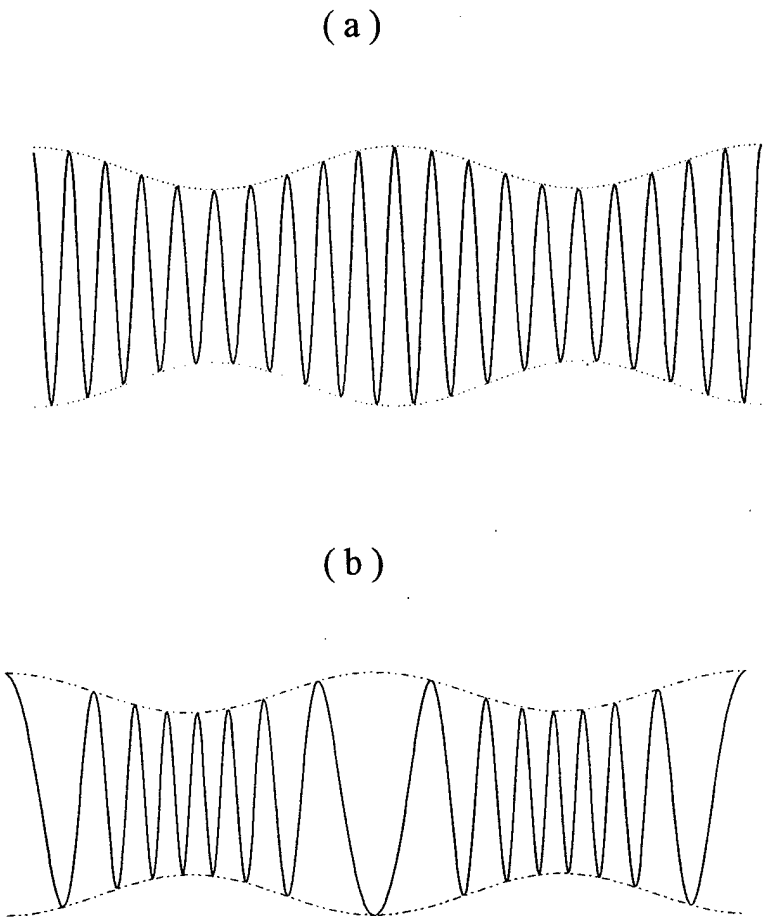

Figure 1. Modulated waves. (a) Initial state of a modulated wave in the frame moving with the group velocity v_g. (b) For positive dispersion, $\omega''(k) > 0$ and $\omega_2 > 0$, dv_g increases toward the troughs of the modulation, and the modulation propagates.

The stability of the modulation has the important consequence of AM-FM conversion. This effect can be physically understood by considering again a modulated wave in a frame moving with the linear group velocity (Figure 2a). Assume that both the dispersion and the nonlinear coefficient ω_2 are positive. Due to nonlinear effects, an observer at a fixed location in this frame would see, after some time, alternating bunching and anti-bunching of the wave crests (Figure 2b). Because dispersive effects cause the energy to approach the troughs of the envelope, for this observer it would appear that at some time later the initial amplitude modulation has become a frequency modulation (Figure 2c). Dispersive effects would again remove energy from the region where the crests are more spread apart to the region where the crests are closer together. For the observer fixed in the frame moving with the group velocity it would appear that an amplitude modulation is superimposed upon the frequency modulated signal (Figure 2d). Nonlinearity will prevent an overshoot of energy flow to the crest of the modulation, and an amplitude modulation 180^{o} out of phase with respect to the original signal results at a later time (Figure 2e). In the frame moving with the group velocity, the process repeats periodically, and an observer in this frame sees that the modulations experience beats. In the laboratory frame if a source is generating an amplitude modulated signal, some distance away it will become frequency modulated. Larraza and Coleman [1] also give a quantitative theory for this effect. They have shown that an amplitude modulated signal with amplitude $\sqrt{e_0}$, modulation amplitude m, modulation frequency Ω, and carrier frequency ω will evolve according to

$$a(x,t) = \sqrt{e_0}\left[1 + m\cos(\Delta x)\cos(\Omega t - \eta x)\right] * \cos\left[k_0 x - \omega t - \frac{2m\omega_o'}{\Omega}\sqrt{\frac{\omega_2 e_0}{\omega_o''}}\,\sin(\Delta x)\cos(\Omega t - \eta x)\right], \qquad (1.3)$$

where $\Delta = \Omega\sqrt{\omega_0''\omega_2 e_0}\,/\,\omega_0'^2$.

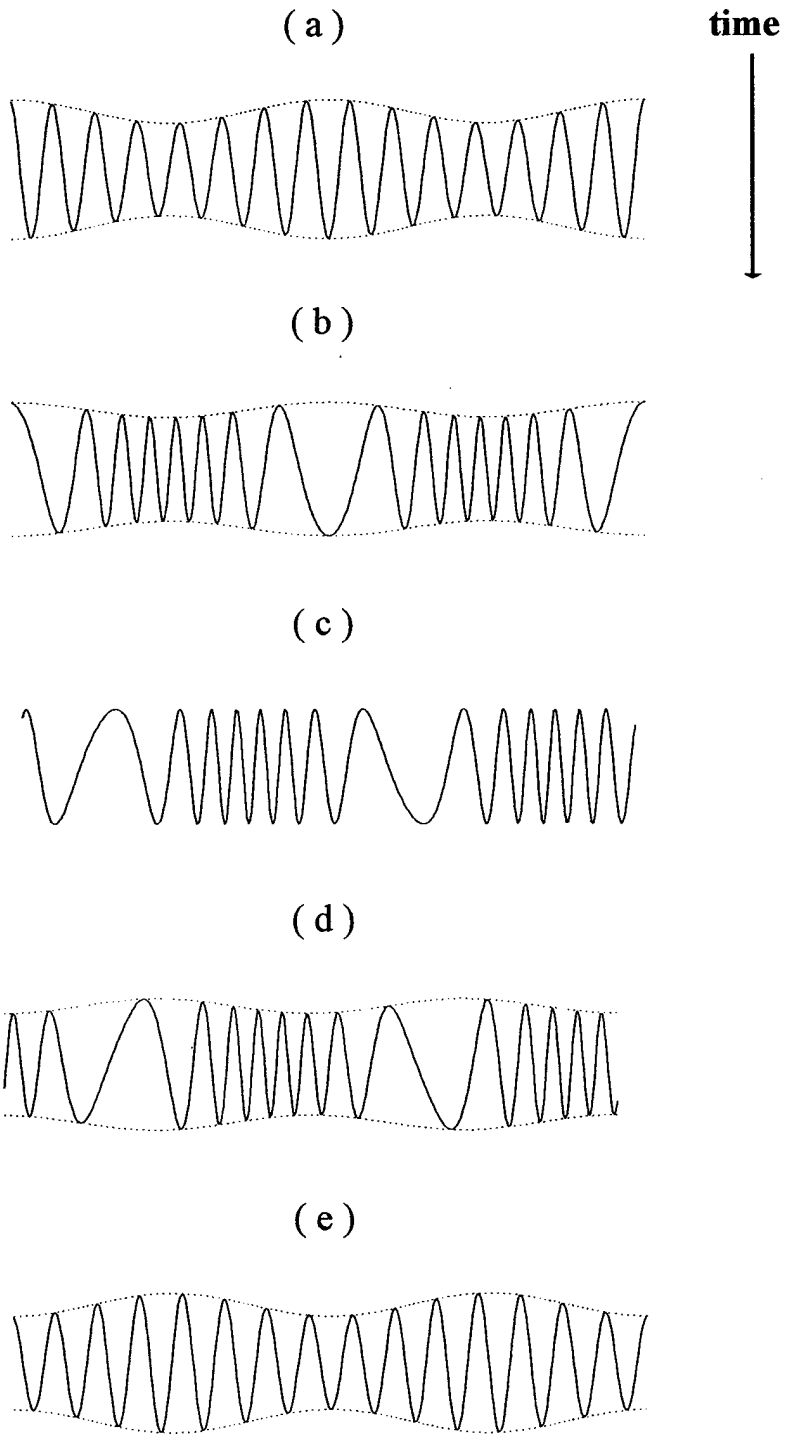

Figure 2. Time evolution of modulation. An observer in a frame moving with the linear group velocity observes AM–FM conversion in time.

A possible application of this result is broadband tunable lasers using fiber optics. Here, we are interested in single mode fibers consisting of a glass core of high index of refraction surrounded by a cladding with a lower index of refraction (about 0.1% smaller). In this case, for light in the visible range the dispersion is normal with $\omega_o''(k) < 0$. For light with intensity I, the index of refraction is given by $n(I) = n_0(\omega) + n_2 I$, where $n_0 \approx 1.5$. Thus, the frequency nonlinear coefficient $\omega_2 \approx -\alpha n_2 \omega_0 / n$ is negative, where α is a numerical factor of order unity. The order of magnitude of the coefficient n_2 (in units of cm^2/W) is typically about 10^{-11} or higher in doped glasses.

Because the product $\omega_o''(k)\omega_2 > 0$, the physical picture presented above applies to this case. In particular, for a 0.1 W source operating at a frequency of 5.8×10^{14} Hz and a 50% amplitude modulation of 10^{10} Hz in a 10 μm^2 fiber, the distance $x_m = \pi/2\Delta$ for AM–FM conversion is about 20 m in doped glasses. The corresponding FM frequency spectrum has a range of about 3.5×10^{14} Hz in doped glasses. Thus, in doped glasses, an amplitude modulated green light alternating between bright and dim at the source will alternate between red and blue at a rate of 10^{10} Hz at a location about 20 m down the fiber. This mechanism allows the possibility of producing tunable phased–locked coherent light from a single frequency coherent source.

The purpose of this thesis research consists of three tasks. First is to evaluate the frequency output of an argon ion laser source in single mode operation at 514.5 nm. The objective is to know precisely how well the laser produces a single mode output. The second task is to evaluate the side bands of that same argon ion laser source when it is amplitude modulated at frequencies of the order of 100 MHz. The objective is to obtain

high enough resolution with a Fabry-Perot interferometer to actually distinguish the AM sidebands from the carrier and thus verify that amplitude modulation behaves as expected. The third task is to measure the attenuation of the green laser light in a typical silica-based optical fiber. This information will all be used in follow-on work towards the ultimate goal of AM-FM light conversion.

Chapter II discusses the set-up of the overall experiment (Figure 3) and describes each component of the experiment in detail. Some preliminary measurements and results are also presented in Chapter II. Chapter III discusses the measurements of the frequency output of the argon ion laser and the search for AM sidebands. Chapter IV discusses fiber optic coupling and the measurement of attenuation.

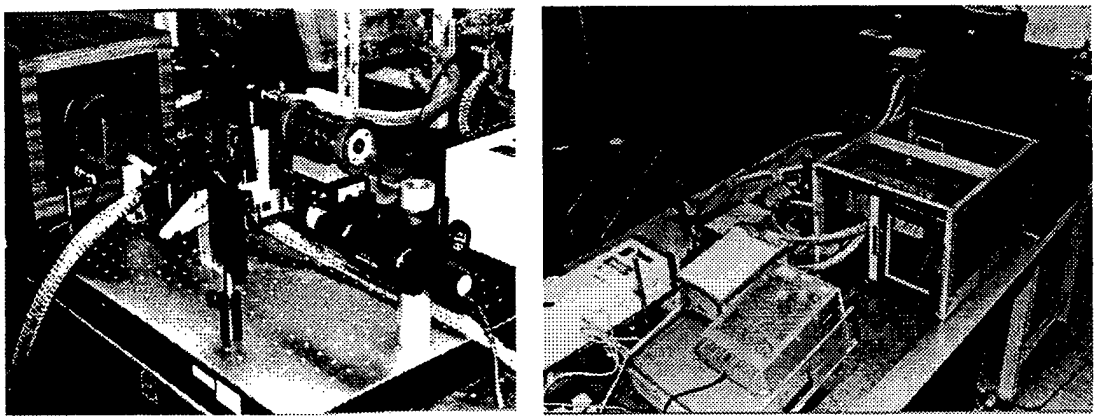

Figure 3. Photographs of the set-up of the experiment. Left: modulator, mirrors and filters, interferometer. Right: laser, power supplies, oscilloscope, power meters.

II. OVERVIEW AND PRELIMINARY MEASUREMENTS

A. INTRODUCTION

This chapter discusses the details of each component of the experiment. Figure 4 shows the overall set-up of the experiment. A continuous wave argon ion laser is used for

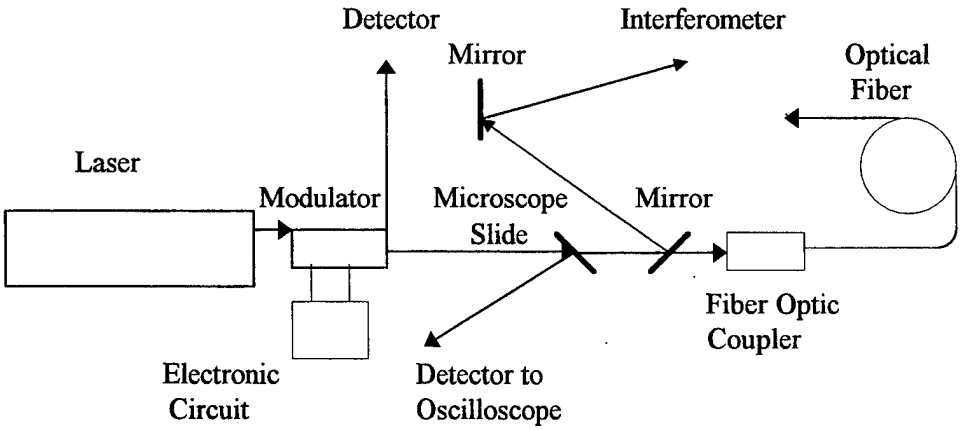

Figure 4. General set-up of experimental components. The modulator, microscope slide, mirror, and fiber optic coupler are all mounted on a rail such that they can be individually removed and replaced.

the light source. The laser beam is directed through an electro-optic modulator for amplitude modulation. A Brewster cube is attached to the exit end of the modulator and acts as a beam splitter sending one beam parallel to the incident beam and a second beam perpendicular to the incident beam. The perpendicular beam is directed into a detector so that the average value of the optical power can be is monitored. Both the frequency of modulation and the amplitude of modulation are determined by the electronic circuit connected to the modulator. The circuit can be tuned to produce different frequencies and amplitudes of modulation. A microscope slide is used to reflect a small portion of the forward beam into a detector whose output is sent to an oscilloscope. The majority of the

beam passes through the microscope slide and is guided to propagate down a fiber optic cable. A mirror can be placed in front of the optical fiber and used with a second mirror to direct the beam through a Fabry-Perot interferometer. The remainder of this chapter discusses the specifics of each of these components.

B. LASER

A LEXEL Model 85 continuous wave argon ion laser (Figure 5) is used for the light source. This model is a class 3b laser. The maximum optical power output was experimentally determined to be approximately 320 mW in single mode operation with a wavelength of 514.5 nm.

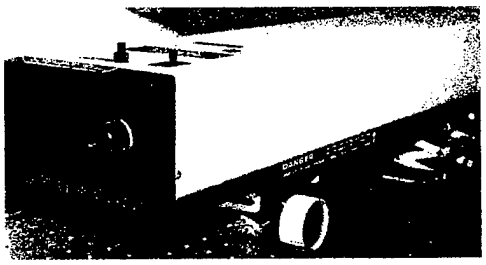

Figure 5a. LEXEL model 85 laser.

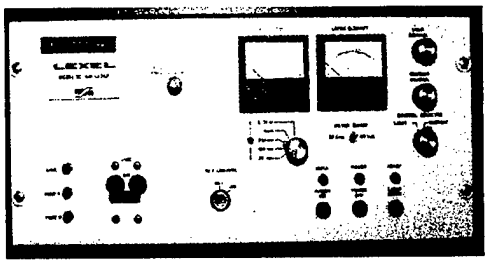

Figure 5b. LEXEL model 85 power supply.

The laser has two operational controls: light control and current control. When the laser is operated in the current control mode, the plasma-tube current is maintained at a selected level. This setting provides a reasonably constant optical power output, but it does not compensate for any minor changes in the optical components, such as thermal variations of cavity length, during operation. This can result in fluctuations in the optical power output. When the laser is operated in the light control mode, a small portion of the laser's output is sampled by a beamsplitter inside the front of the laser head. This sampled light is detected by a silicon photocell, and an electrical voltage proportional to the

intensity of the light is fed back to a regulatory circuit. A differential amplifier in the regulator compares this voltage with a reference voltage that is set by the light control potentiometer, and an error signal proportional to the difference between the two is generated. The error signal is amplified to drive the power transistors in the regulator passbank, causing them to increase or decrease the plasma-tube current as required to maintain the output beam at a constant output power [2]. In light control mode, the plasma-tube current may vary considerably. In general, the light control provides a very steady optical power output that is considerably more stable than that provided by current control mode.

The laser output was experimentally confirmed to be linearly polarized with the electric field in the vertical direction, that is, perpendicular to the optical table. The beam diameter was experimentally determined to be approximately 1.2 mm (Figure 6). This was

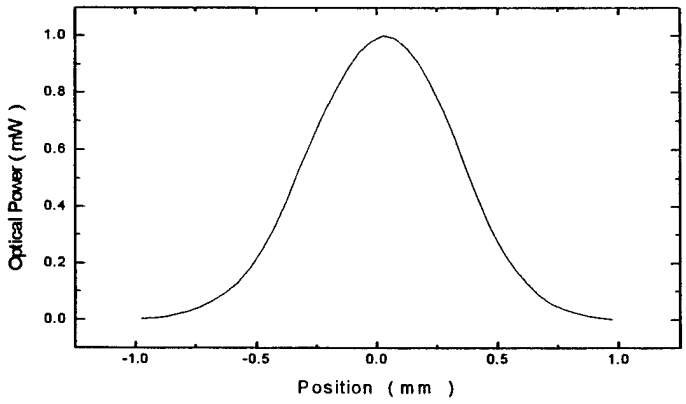

Figure 6. Plot of laser beam power as a function of transverse position. Beam profile is approximately Gaussian with a width of approximately 1.2 mm.

done by painting one side of a microscope slide flat black and then scoring a slit in the paint with a razor blade and straight edge. The slit was then passed through the beam and

back again both in a direction parallel to the table and a direction perpendicular to the table. Measurements of position were recorded using a micrometer tool. This provided four sets of data with which to plot position versus optical power. An average of the four sets of data is plotted in Figure 6. The laser specifications list the beam diameter as 1.1 mm.

C. MODULATOR

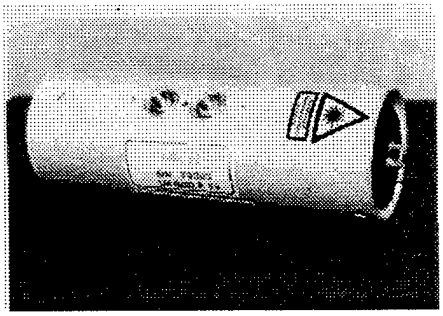

Figure 7. LM0202P Electro-optic modulator. The input aperture is 3 x 3 mm square. A Brewster cube is mounted to the exit end. Microdot connectors are used to apply voltage.

A Gsänger model LM0202P intensity modulator was used to amplitude modulate the continuous wave laser beam source. The LM0202P takes advantage of the linear electro-optical phenomenon known as the Pockels effect. This effect is a temporary double refraction induced in many solids by application of an electric field. The applied electric field causes a shift in the material's anisotropic index of refraction which in turn causes a modification of the relative phases of different polarization modes. Controlling the polarization of the laser light electronically can lead to amplitude modulation when the resulting beams traverse polarizing elements. The LM0202P has a Brewster cube attached to the exit end of the modulator which is the single polarizing element necessary as analyzer.

The LM0202P uses four KDP crystals, in series optically and in parallel electrically. The crystals must be oriented in a particular position relative to incident polarized light in order for proper amplitude modulation to occur. Consider a standard x, y, z coordinate system where z is in the direction of propagation of the laser beam and x, y are oriented along the crystal's principle axes. If an electric field is applied along the z axis of the crystals, then the x, y optical axes are rotated to a new position x', y'. This changes the relative position between the plane of polarization of the light source and the optical crystal's axes. This change in relative position causes a modification in the phase between the two polarization modes as described above. When the electric field of a linearly polarized light source is oriented 45 degrees from the optical axes of the crystals and with no voltage applied, the modulator will act as a quarter waveplate and change the linear polarization to circular.

As the voltage applied to the modulator is increased from zero, the net phase shift between the two components will generally result in elliptically polarized light due to the change in relative position between the plane of polarization of the light source as described above. At some point, the phase changed induced by the applied voltage will be $\pi/2$ and the polarization will once again become circular. The Brewster cube splits the two components of the circularly polarized light. One is sent in the same direction of propagation but is now oriented with its plane of polarization in the horizontal direction parallel to the optical table. The other is sent perpendicular to the direction of propagation but keeps its orientation with the plane of polarization in the vertical direction perpendicular to the table (Figure 8). When the voltage applied results in elliptically polarized light, the components are separated by the Brewster cube and the two exiting

beams are unequal in magnitude. If aligned as described above, the LM0202P will therefore change linearly polarized light into circularly polarized light with no voltage applied and then again at some specific value of voltage. That value was experimentally determined to be 165 V by incrementally increasing voltage applied to the modulator and recording the optical power of each beam exiting the Brewster cube (Figure 9).

There remains some concern as to whether or not this is indeed the proper way to align the modulator. It is evident from Figure 9 that the DC characterization curve is not symmetric and this is a point of concern. It is considered that the correct alignment may possibly be for maximum transmission in the perpendicular beam and minimum transmission in the forward beam. Nevertheless, the curve in Figure 9 was reproducible time and time again. The data for Figure 9 was taken with 68 mW of input into the modulator and 30 mW of output from each beam exiting the Brewster cube for an overall transmission of approximately 88% with 0 volts DC. Both spots were crisp and clear.

At 165 V, the horizontal and vertical components of the exiting beam are equal in magnitude. The result is two perpendicular beams of light equal in optical power exiting the Brewster cube. At 85 V, there is extinction in the direction of propagation and transmission in the direction perpendicular to propagation. At 255 V, the reverse occurs with transmission in the direction of propagation.

An alternating voltage that ranges from 85 to 255 V applied to the modulator results in 100% amplitude modulation. A greater range results in over-modulation and distortion. Data taken with a modulation frequency of 1 kHz at different ranges of voltage shows these three conditions (Figure 10).

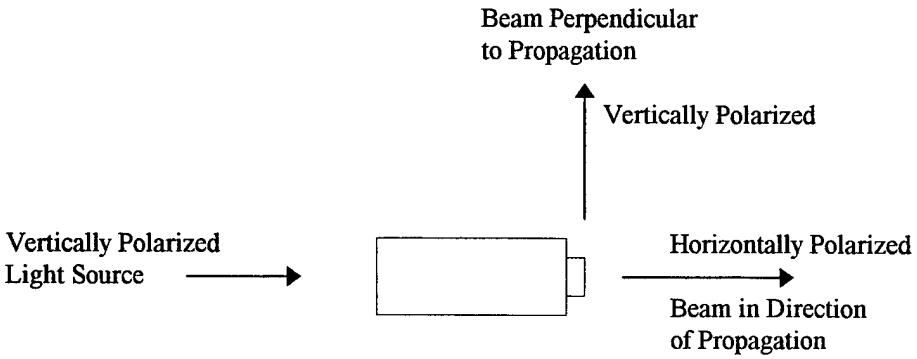

Figure 8. Effect of Brewster cube at exit end of modulator.

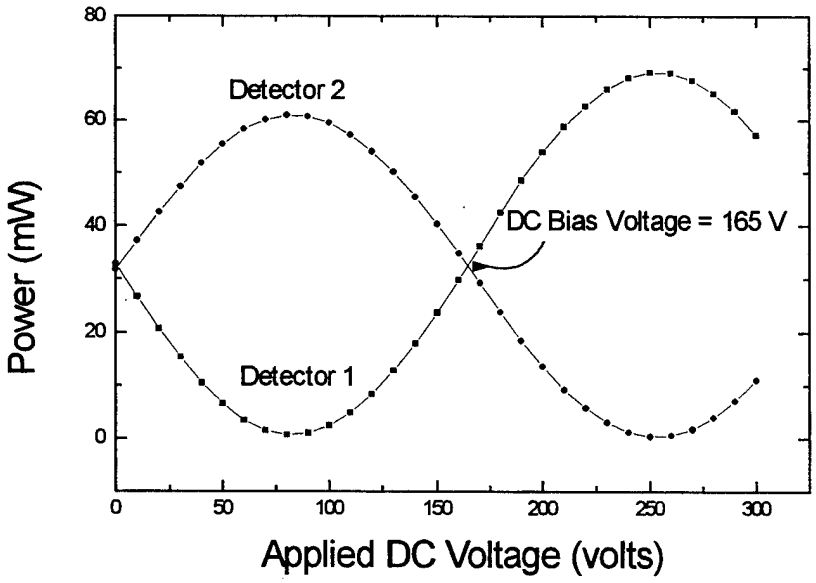

Figure 9. Applied DC voltage versus optical power output for LM0202P intensity modulator.

(a)

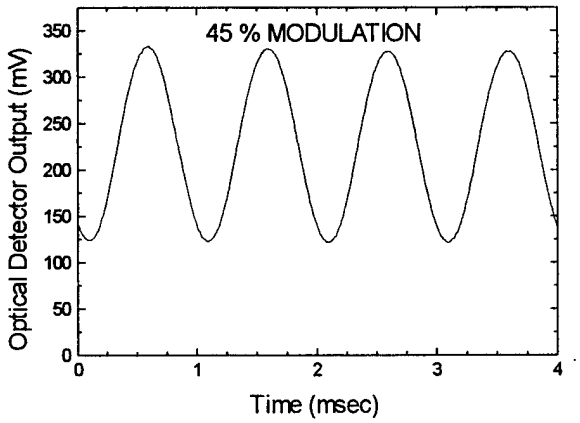

(b)

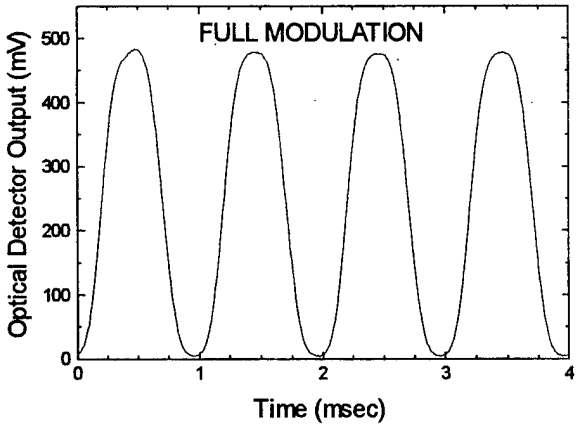

(c)

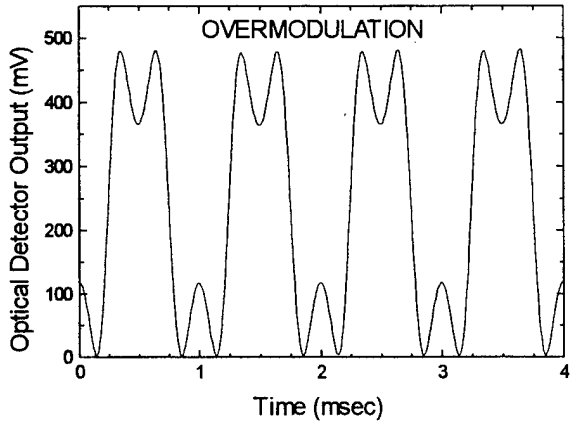

Figure 10. Representative outputs of modulator at various voltages. Shown are outputs for AC voltages (a) 57 V_{pp} (b) 165 V_{pp} (c) 284 V_{pp} [3].

The electro-optical properties of the crystals in the modulator are extremely temperature sensitive. Experimental results are most consistent when the laser is run through the modulator for approximately one half hour before any voltage is applied. It is best to wait nearly that long again after applying DC voltage to allow the optical output to stabilize before applying any AC voltage. AC voltage causes dramatic thermal fluctuations every time that it is applied to the modulator. After the fluctuations settle, the DC voltage must once again be adjusted in order to obtain circular polarization and equal magnitude in the beams exiting the Brewster cube.

D. ELECTRONIC DRIVING CIRCUIT

The modulator was initially thought to act as a capacitor element. The capacitance was measured to be approximately 82 pF. This is true, however, only with very short (half an inch or less) leads to the pin connections of the modulator. As soon as any connections at all were made between an electronic driving circuit and the modulator, inductive loops were produced and the modulator no longer acted as a simple capacitor. This problem proved extremely difficult to address, and in the end an entire separate thesis was conducted to characterize and to understand the electronic operation of the LM0202P modulator. Three separate circuit designs were constructed and tested in the research. A summary of each design and the results of the testing make up the rest of this section. The third and final design was the one used to drive the modulator for the final results of this thesis.

It was originally decided to drive the modulator through a tuned radio frequency transformer with both the primary and secondary circuits tuned to the working frequency. It turned out, however, that the Q-factor of the secondary circuit was not sufficiently high

to boost the output voltage to 160 Vpp, and it became necessary to make use of a RF amplifier to enhance the voltage supplied by the signal generator. Note that the arrangement includes provision for applying a DC voltage to the modulator in addition to the RF voltage. This allows the adjustment of the bias voltage to ensure that the modulator operated at the 50% transmission point for symmetrical modulation. The purpose of the 0.01μF capacitor is to ensure that the bottom end of the secondary is at AC ground while being at an elevated DC voltage. The 100 kΩ resistor protects the DC power supply from an accidental short circuit [3].

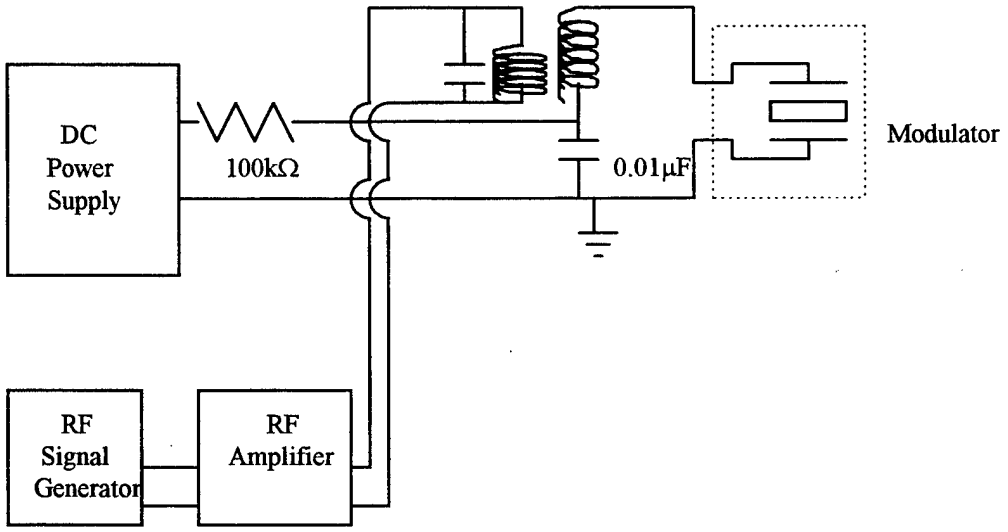

Figure 11. Equipment setup for transformer action [3].

Separate transformers were wound with different numbers of secondary turns to resonate at different frequencies. They were tested with an 82 pF capacitor before being used to drive the modulator. In each case, the primary turns were adjusted for maximum secondary voltage at resonance. Satisfactory results were obtained up to 20 MHz. Above

that frequency, however, a transformer could not be used because the required number of turns in the primary and secondary windings was so low that there was a severe mismatch between the primary impedance and the output impedance of the amplifier. The transformer was therefore replaced by a parallel tuned circuit [3].

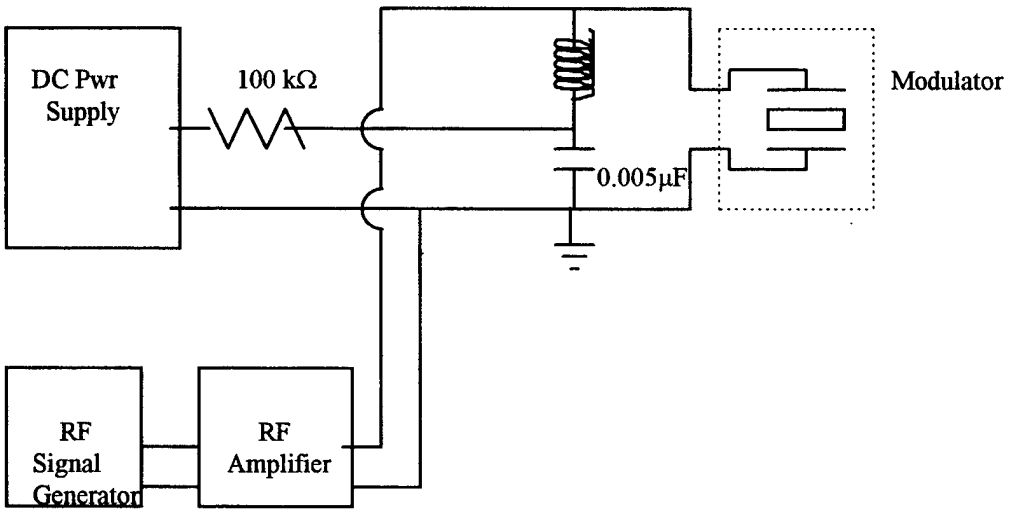

Figure 12. Parallel tuned circuit [3].

The resonant frequency of the parallel tuned circuit was varied through proper selection of the inductor with or without a parallel capacitor. The equipment setup, with appropriate RF screening methods, remained the same as that used for lower frequencies which made use of a transformer. The 0.0050 μF capacitor provides an AC ground while allowing the use of the DC bias. The 100 kΩ resistor is present again to protect the DC power supply from an accidental short circuit. The RF amplifier with a maximum power output of 4 W (into a 50 Ω load) could not supply a voltage greater than 40 V_{pp} to the parallel tuned circuit [3].

A third arrangement was developed where the DC and RF voltages were both supplied through the same coaxial cable with the help of a hybrid circuit. The hybrid circuit could drive the modulator through a coaxial cable connected to one of the SMC connectors on the modulator, with the other SMC connector grounded. This arrangement precluded the use of an inductor to resonate with the crystal capacitor. Nor did it make it possible to measure and regulate the RF voltage at the modulator terminals so as to determine the true frequency response of the modulator. But it did eliminate the inductive loop in the external open connections to the modulator [3].

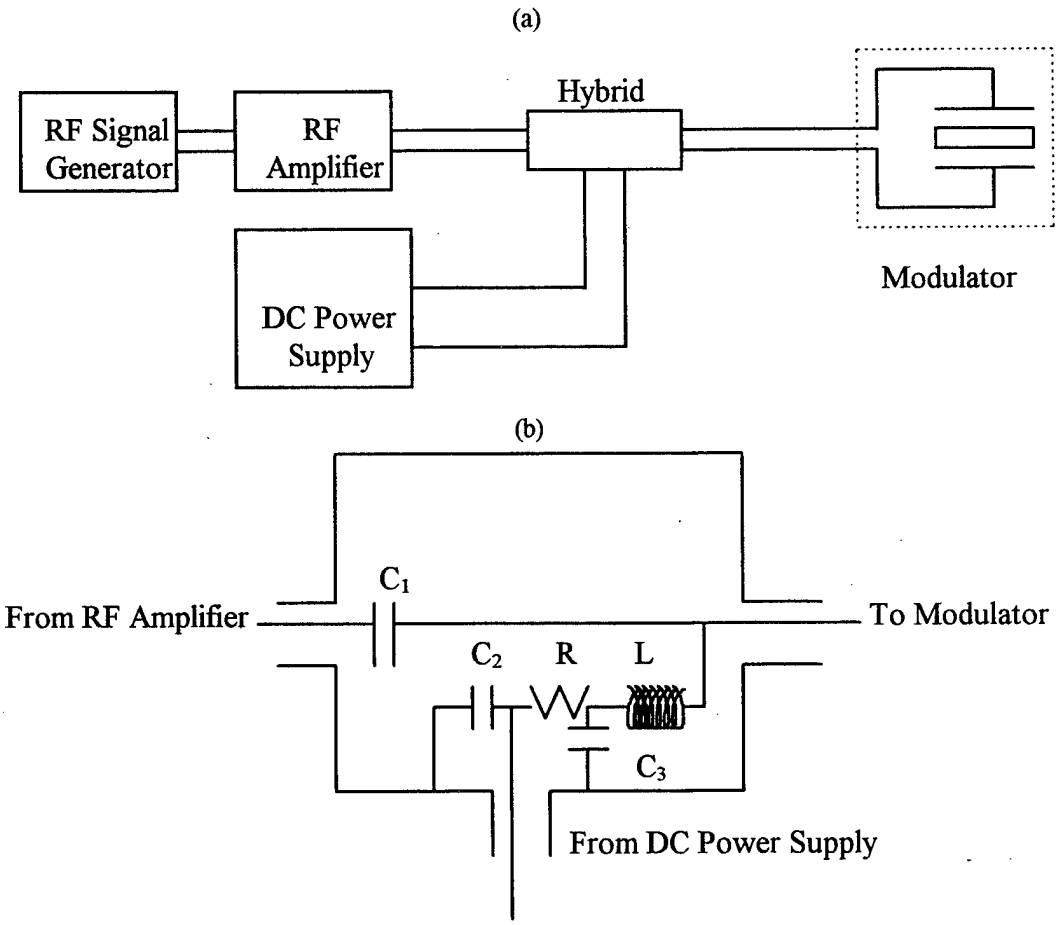

Figure 13. Setup. (a) Equipment set-up with no RF voltage monitoring. *Connections between components are via coaxial cable.* (b) Close up of hybrid connector. C_1 = 0.01 μF 500V, C_2 and C_3 = 0.0047 μF 500V, R = 100 kΩ 1/2 W, L = RF choke 1 μH [3].

E. DETECTORS AND POWER METERS

A Coherent Model 205 power meter and sensor is used to determine the maximum optical power output of the laser and for start-up each time the laser is used. It is mounted to the table such that it can be easily swung in front of the laser to act as a "laser light dump" while adjustments are being made. The sensor is a thermal disc whose maximum intensity rating is 200 W/cm^2. The response time of this detector is less than one second.

Two identical detectors with power meters are used to measure the optical power output of the perpendicular beams from the Brewster cube at the end of the modulator. These are Newport model 815 power meters and model 818-SL detectors. The detectors each have a neutral density filter of density factor 3, which allows for input up to 2 W/cm^2. The power meters also have an output connection that allows the signal to be sent to an oscilloscope. In this way, the peak-to-peak amplitude modulation can be measured accurately.

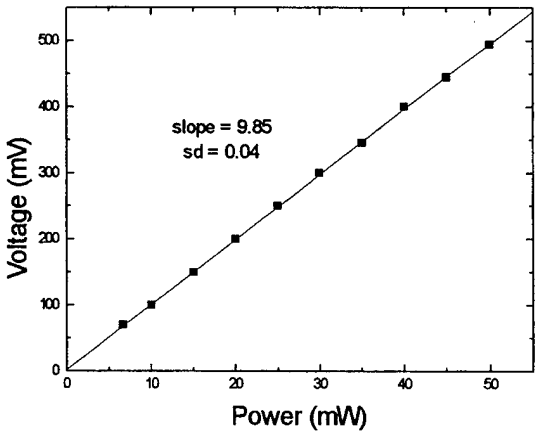

Figure 14. Response curve for Newport detector. The voltage is measured with an oscilloscope from the analog output of the detector. Power is controlled via the laser power supply.

The Newport detectors use a silicon diode with a rise time of 2 μs. This leads to a theoretical maximum response time of 500 kHz. Beyond 500 kHz, the detectors can only be used as power meters because they effectively average the time-varying incident flux.

A series PD30 ultra high speed photodetector with PS30 power supply from Opto-Electronics Incorporated is used for experiments at frequencies above 100 kHz. The detector was experimentally tested for accurate response up to 250 MHz. It uses an avalanche silicon photodiode with a rating of 100 mW of average optical power. The detector is designed for use with the power supply operating at approximately 100 μA of bias current, where the diode current-voltage curve is approximately linear with a maximum power supply current of 200 μA. As Figure 15 shows, experimental data taken with 100 μA of current through the power supply exhibits an approximately linear behavior.

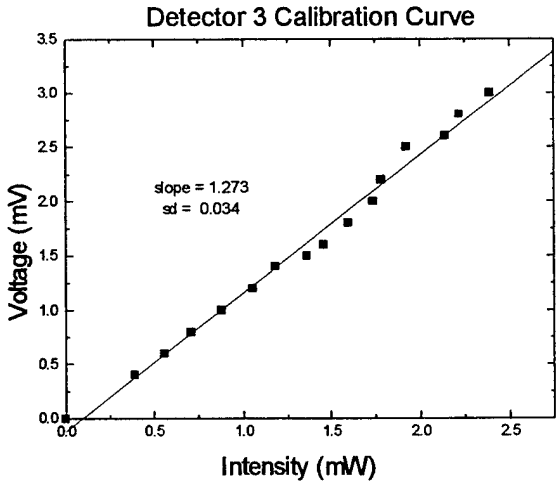

Figure 15. Calibration curve for PD30 ultra high speed photodedector. Throughout the experimental work, this detector was referred to as detector three. The Newport detectors were designated as one and two.

A microscope slide is used to reflect a fraction of the modulated beam into the high speed detector. A device was constructed to aim the reflected beam into the small aperture of the detector. The microscope slide is hung from an arm that is attached to a control that allows for precise rotation of the arm (Figure 16). This rotates the slide in a plane perpendicular to the table and adjusts the reflection vertically up and down along the face of the detector. This rotation stage with the attached arm is mounted to a post that fits in a holder which allows the post to rotate which in turn rotates the slide parallel to the table. This provides adjustments of the reflection horizontally from side to side along the face of the detector. The device is braced to reduce vibrations, and neoprene spacers are used to dampen vibrations in order to maintain a steady reflection from the slide.

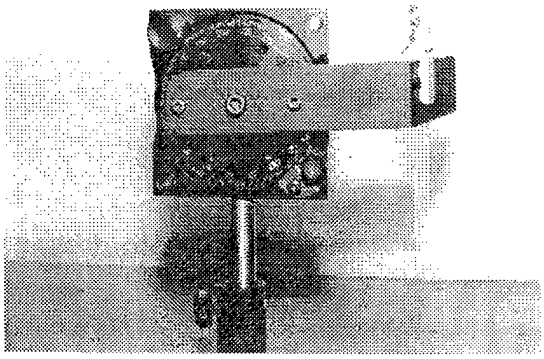

Figure 16. Microscope slide reflector.

F. ALIGNMENT

As in any optical set-up, the key to success with this experiment is careful alignment. The laser sits on two large lab jacks which provide initial macroscopic changes in the height and tilt of the beam. The modulator and fiber optic coupler mount to a rail which is fixed to the table in front of the laser with the center line parallel to the beam.

Each component on the rail can be removed and replaced at any time. Most of the optical mounts are combinations of New Focus and Newport equipment.

A New Focus Model 9082 five-axis aligner is used for the base support of the modulator in order to align the beam through the tube. Four of the adjustments combine for tilt or pivot about the center of the base and also translation vertically or horizontally perpendicular to the beam. The fifth adjustment allows for horizontal translation parallel to the beam and is not actually necessary. A mounting had to be designed that would both hold the modulator fixed on the five-axis aligner and that would allow azimuthal rotation about the long axis of the modulator.

A plastic tubular sleeve was fitted over the modulator. A second sleeve of shorter length was then fitted over the first sleeve. This allowed end ring clamps to be used to both tighten the inside ring snugly against the modulator and to prevent the inner tube from moving longitudinally relative to outer tube. The modulator is rotated by grasping an end ring and rotating that ring which results in the rotation of also the inner sleeve and modulator. There is sufficient friction between the inner and the outer sleeve to hold the modulator in place after rotation is complete and the desired position is established.

The plastic sleeves had to be drilled with several holes to allow for cooling of the modulator. The modulator is encased in aluminum to help minimize thermal effects that would cause the crystals to expand and contract, thereby changing the optical path. A fan was used to blow air across the modulator and this air was able to reach the aluminum casing through the drilled holes.

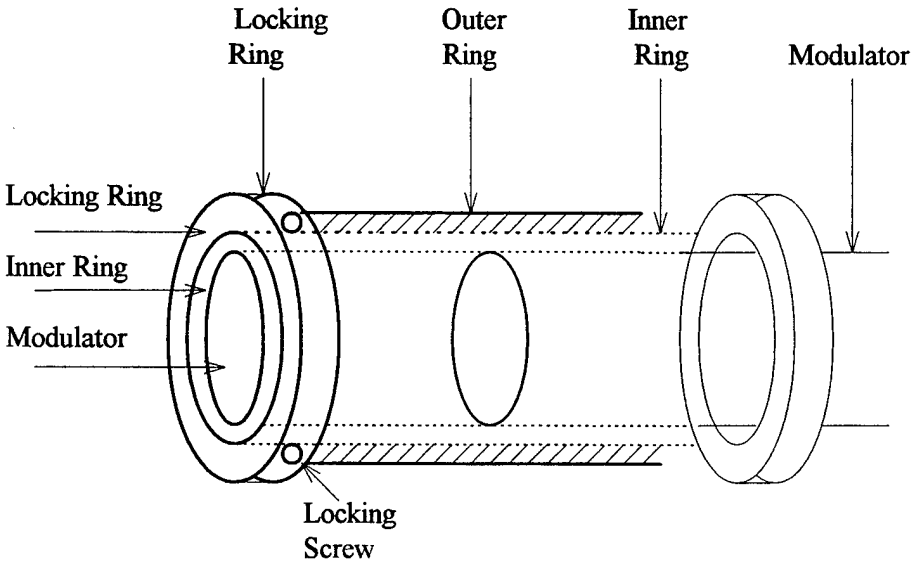

Figure 17a. Exploded view of mounting for azimuthal rotation about the long axis of the modulator.

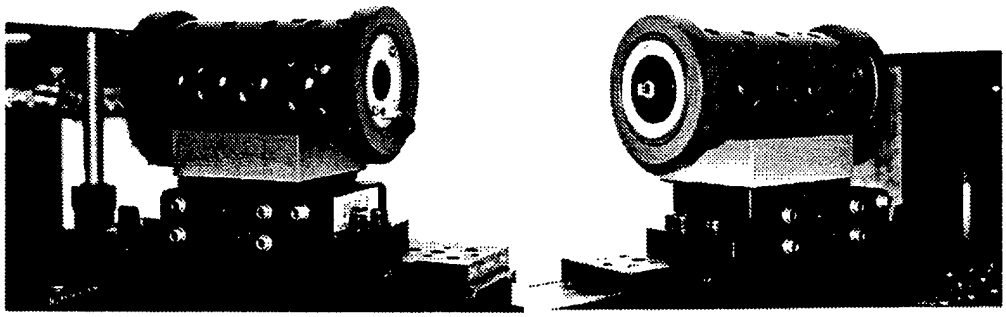

Figure 17b. Photographs of modulator fixed to complete alignment mounting. Left: entrance end of modulator with ground connection. Right: exit end of modulator with Brewster cube.

The next challenge in the alignment process was the mounting for the fiber optic cable. The laser beam is focused into the fiber optic cable with a microscope objective lens. It is critical that the beam hit the aperture of this lens on center and perpendicular to the lens. The height of the beam is fixed once alignment through the modulator is established. Therefore, it is required to make the mounting for the objective lens such that

the center of the lens can be physically moved into the beam while allowing alignment that is also perpendicular to the beam.

The mounting that is used for the microscope objective lens is a Newport F-916 series fiber coupler. The fiber coupler attaches to a Newport base that allows for small adjustments either in the tilt or pivot (two-axis alignment) of the lens compared to the beam, but not for translation vertical or parallel to the table. The Newport base was replaced with a New Focus model 9071 four-axis aligner to allow vertical and horizontal translation as well as tilt and pivot. A spacer was fabricated to place the fiber coupler in the approximately correct position and was also utilized to connect the mechanically incompatible Newport and New Focus parts.

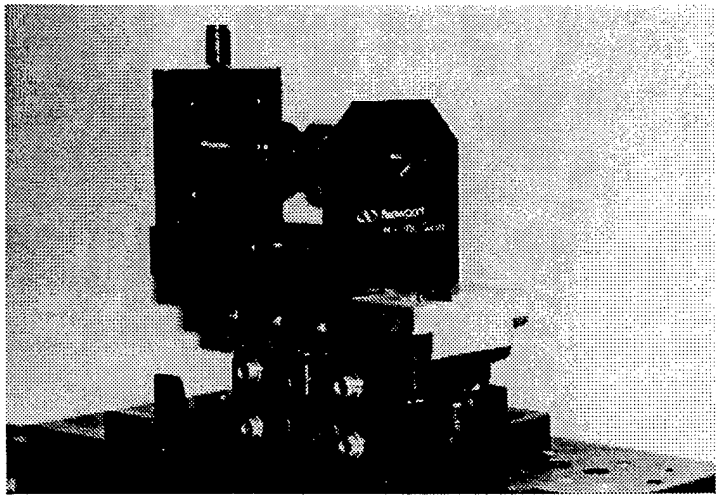

Figure 18. Newport fiber coupler with New Focus four-axis aligner attached to rail.

The final and most interesting alignment challenge came in directing the beam through the Fabry-Perot interferometer. A second device similar to the one described previously for holding the microscope slide (Figure 16) was built. Mirrors were attached to the arms of each device. The beam was reflected from one mirror to the other and

through the interferometer. By simultaneously adjusting both mirrors, the height and slope of the beam as well as the horizontal path of the beam were easily controlled. In this manner, the beam was directed through the center of the Fabry-Perot and perpendicular to its optical elements.

G. FABRY-PEROT INTERFEROMETER

A Tropel model 360 Fabry-Perot interferometer and Tropel model 361 Fabry-Perot controller were used in the experiments. The Fabry-Perot interferometer is a multiple-beam interferometer. The two glass plates that make the etalon spacing are coated on the inner surfaces such that an incoming wave is reflected many times between the two surfaces. An interference pattern is produced as in two-beam interference; however, as the number of interfering beams increases by reflections back and forth in the etalon, the fringes become sharper. With a monochromatic broad diffuse source, the interference fringes will be narrow concentric rings, corresponding to the multiple beam transmission pattern. The position of the fringes depends upon the wavelength. That is, each wavelength gives a separate fringe pattern [4].

The Fabry-Perot interferometer can be used to resolve very close wavelengths into separate fringe patterns. The resolving power is determined by

$$\Re = F\left(\frac{2nd}{\lambda}\right), \qquad (2.1)$$

where $F = \pi R/(1-R)$ is known as the finesse, n is the refractive index between the mirrors, d is the distance between the mirrors, and R is the reflection coefficient of the mirrors. For nd of 10 cm, R of .9 and λ of 514.5 nm, the resolving power is on the order of 10^7.

III. LASER OUTPUT SPECTRUM AND SEARCH FOR AM SIDEBANDS

A. OUTPUT SPECTRUM OF LEXEL 85 ARGON ION LASER

To determine the frequency structure of the laser, the Fabry-Perot interferometer is illuminated with a collimated laser beam, and all the light transmitted through the Fabry-Perot is focused on a detector, whose output is displayed on an oscilloscope. One of the two etalon plates is on a piezoelectric mirror mount. As the voltage to the piezoelectric crystal is varied, the etalon separation is varied. The light output as a function of plate separation gives the spectral frequency content of the laser source [4].

One of the Newport model 815-SL detectors was used with a Hewlett-Packard model 35670A Dynamic Signal Analyzer to record the spectral frequency content of the LEXEL model 85 argon ion laser. Figures 19-28 present plots of detector voltage versus frequency for the data collected. Both scales are relative. The frequency difference between corresponding portions of the line profile in neighboring spectral orders is calculated from the measured etalon spacing. That is, the free spectral range is

$$\mathrm{FSR} = \frac{c}{2nd} \quad , \qquad (3.1)$$

where n is the refractive index of air and d is the etalon spacing. The measurementst were done with an etalon spacing of approximately 9.32 cm, the free spectral range is approximately 1.61 GHz. This value can be used to interpolate each profile's frequency structure from the plots. Figures 19 and 20 of this section show plots of the laser spectrum, unaffected by any other optics.

It is evident form these plots that the output of the laser is certainly not single

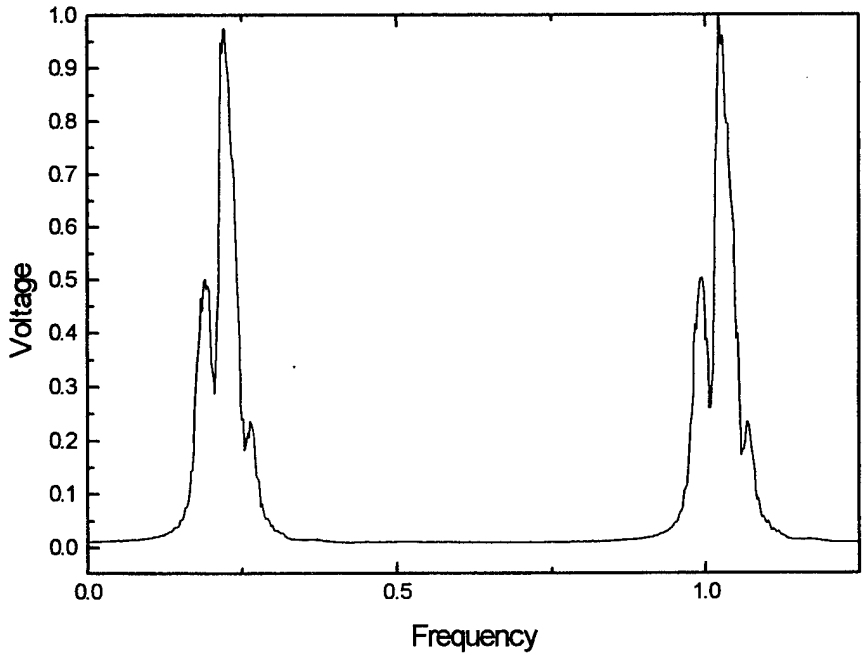

Figure 19. Scan of entire free spectral range from laser. Variations from order to order are artifices of discrete sampling by the Hewlett-Packard analyzer.

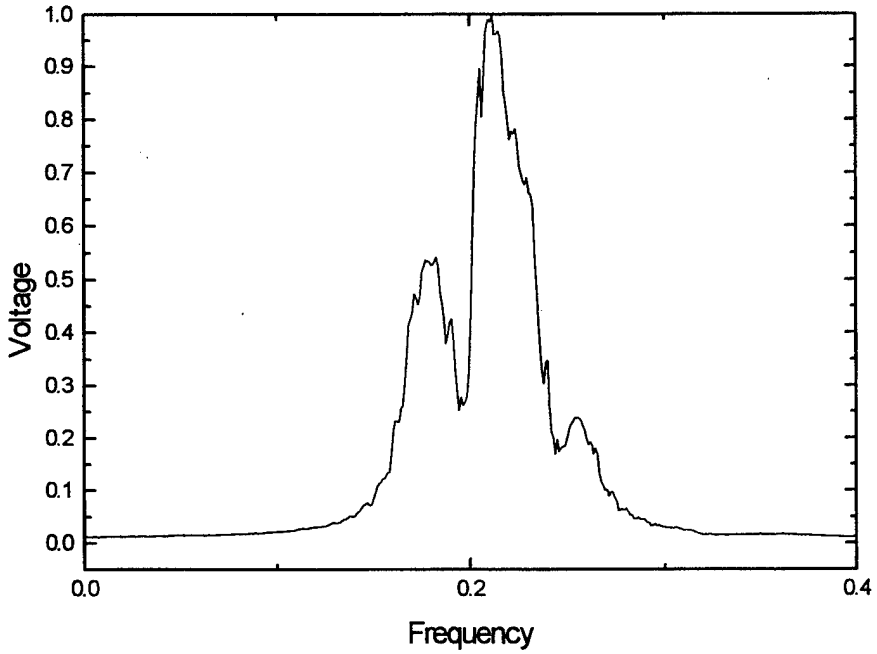

Figure 20. Detail of unmodulated line profile directly from laser.

mode. The laser line profile typically shows three simultaneous modes with a spacing of approximately 50 MHz. This profile was observed continuously for several hours and appears to be relatively stable in time. Therefore, any search for modulator-induced effects must assume this complicated laser line structure as a base.

B. EFFECT OF LM0202P MODULATOR ON LASER SPECTRUM

Insertion of the modulator into the optical path of the beam, with no voltage applied to the modulator, caused a dramatic change in the spectrum. Additional structure was added to the base line structure and the valleys between the three original modes were filled. As DC bias voltage was applied to the modulator, additional spectral changes were noticeable. Examples are presented in Figures 21-24. This makes the base profile even more complex, and complicates the search for AM sidebands.

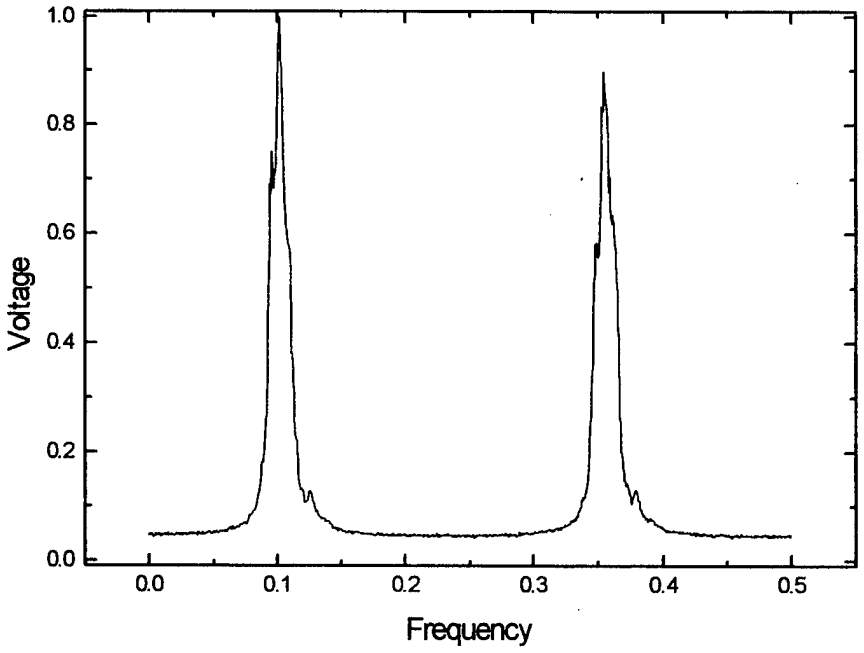

Figure 21. Spectrum exiting modulator with 40 volts DC bias applied to modulator.

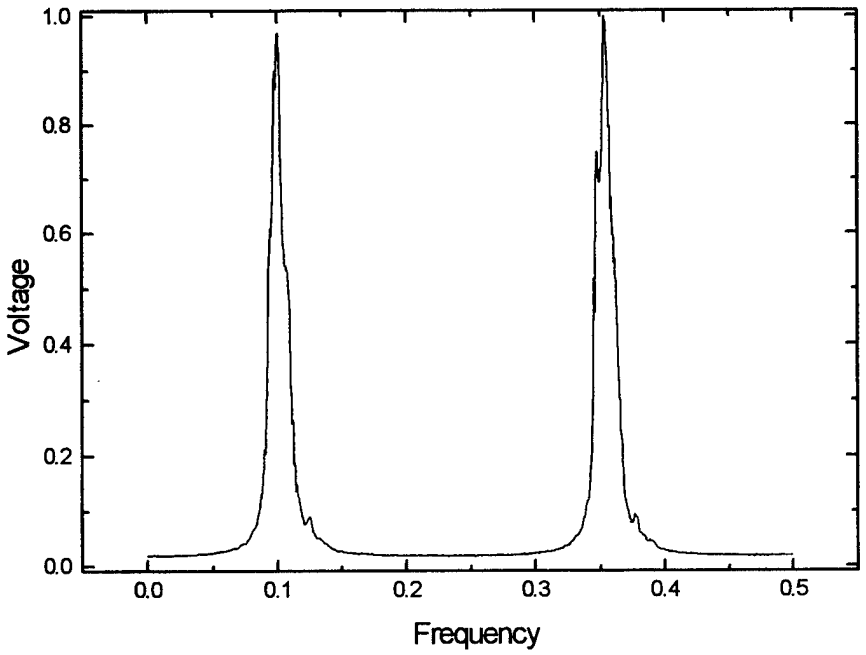

Figure 22. Spectrum exiting modulator with 80 volts DC bias applied to modulator.

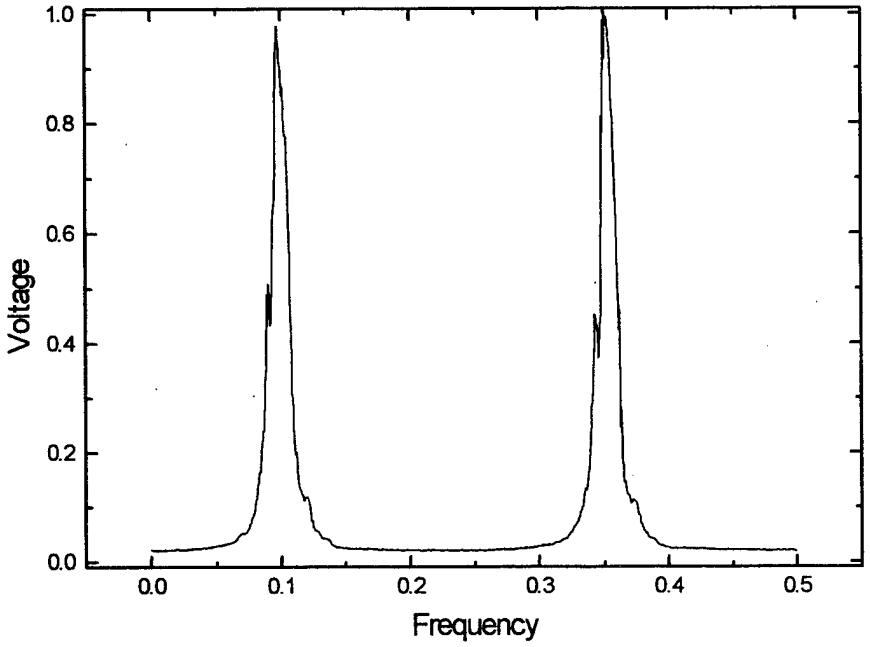

Figure 23. Spectrum exiting modulator with 100 volts DC bias applied to modulator.

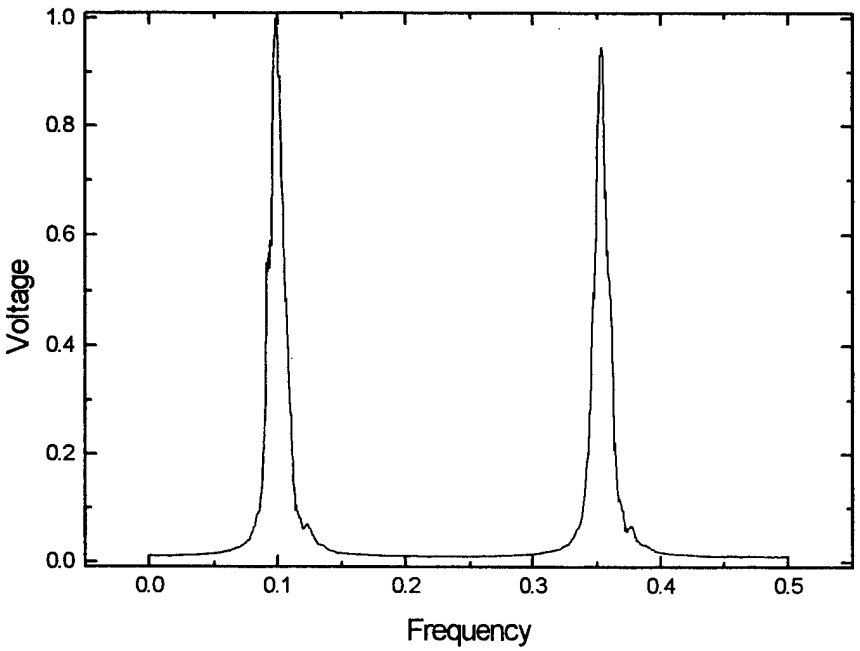

Figure 24. Spectrum exiting modulator with 180 volts DC bias applied to modulator.

C. SEARCH FOR AM SIDEBANDS

Finally, AC modulation was superimposed on the DC bias voltage. This yielded evidence of complicated sideband structure (Figures 25-28). However, the observed structure did not look as expected, even when the complicated base line profile discussed above was taken into account. The modulated profiles are difficult to decipher and seem to make little sense. For instance, it is known that the modulator produces a nice sinusoidal amplitude modulation, as verified directly with an oscilloscope. This modulation should produce a single symmetric pair of sidebands. However, it is evident from Figures 25-28 that the sideband distribution is asymmetric. At the time of this writing, both the cause of the asymmetry and the overall modulated profile are not well understood. Extensive follow-on research will be required to address these issues.

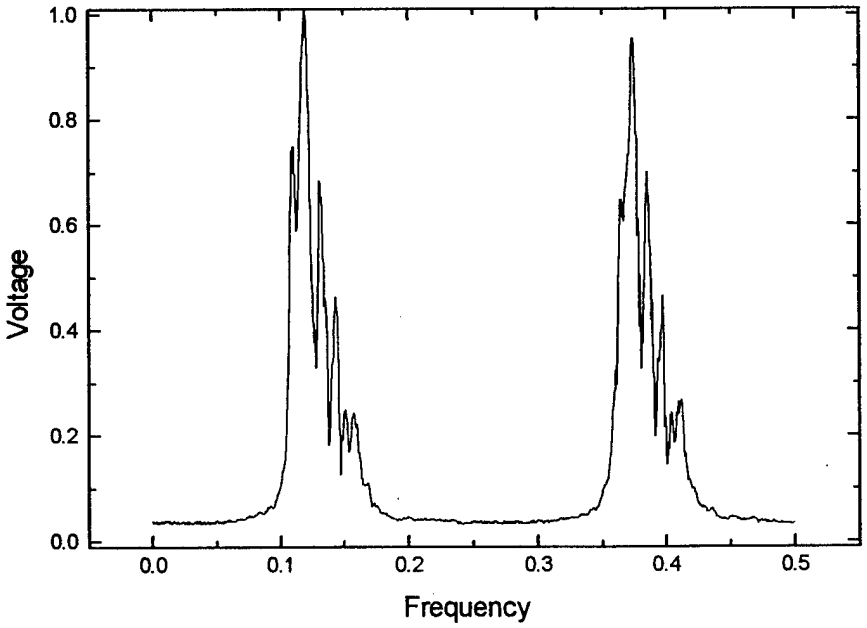

Figure 25. Spectrum modulated at 125 MHz with 20 volts DC bias applied to the modulator and a superimposed AC amplitude of unknown value, resulting in a measured 25 % optical modulation.

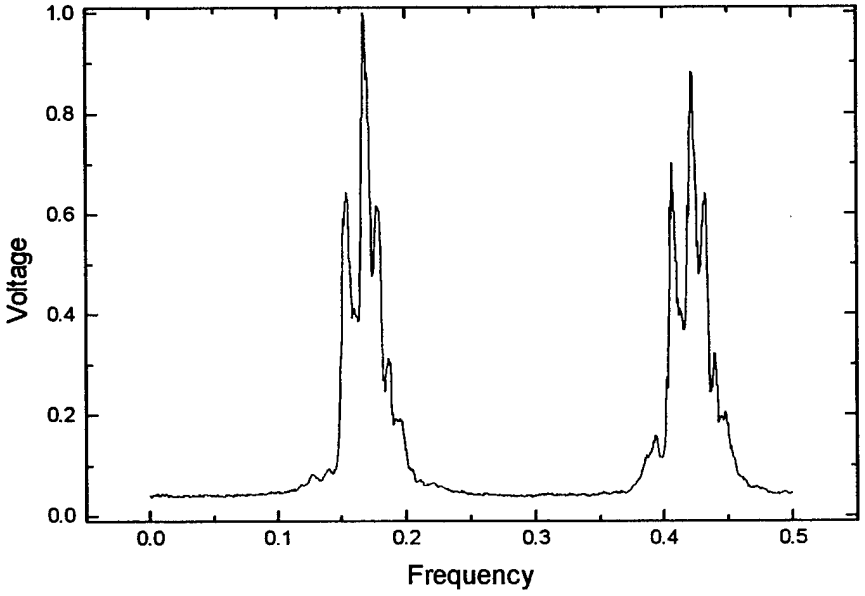

Figure 26. Spectrum modulated at 125 MHz with 180 volts DC bias applied to the modulator and a superimposed AC amplitude of unknown value, resulting in a measured 25 % optical modulation.

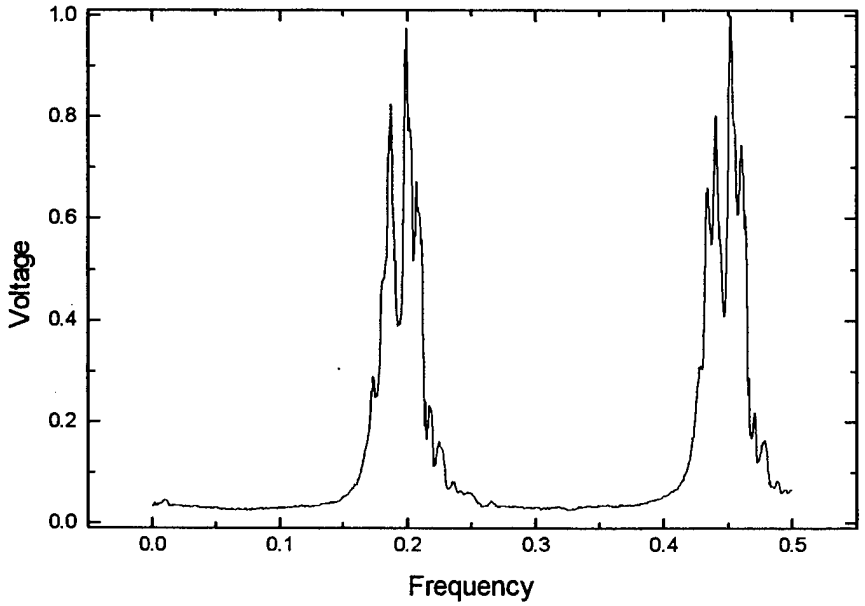

Figure 27. Spectrum modulated at 36 MHz with 0 volts DC bias applied to the modulator and a superimposed AC amplitude of unknown value, resulting in a measured 63% optical modulation.

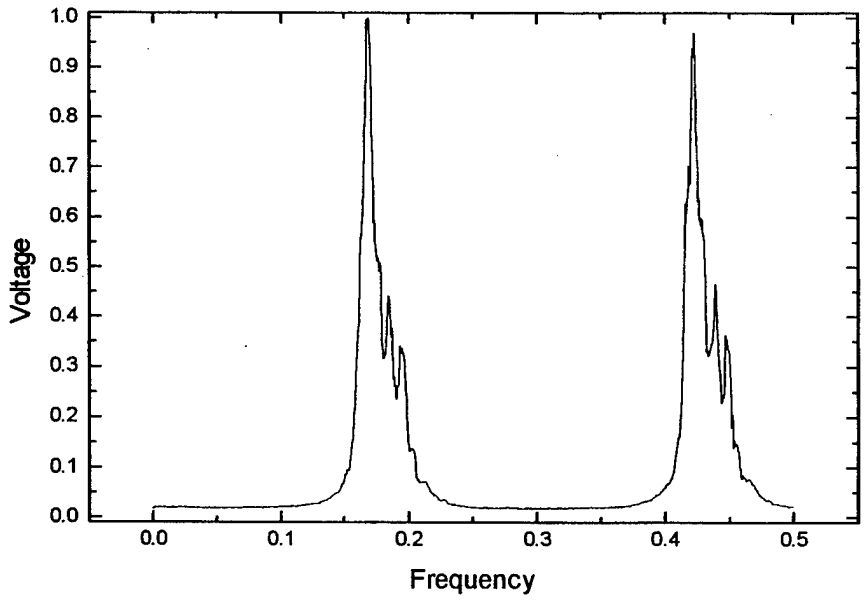

Figure 28. Spectrum modulated at 36 MHz with 170 volts DC bias applied to the modulator and a superimposed AC amplitude of unknown value, resulting in a measured 63% optical modulation.

IV. FIBER OPTIC COUPLING

A. INTRODUCTION

There are three primary considerations to effectively launch a collimated light source down a fiber optic cable. The first is to focus the beam to form a cone of specific size and shape. The second is to properly cleave the end of the optical fiber so that it is flat and perpendicular without any cracks in the glass. The third is to position the center of the end of the optical fiber at the focal point, which is the apex of the cone. These three steps combine to allow the full cone of light to enter and propagate down the optical fiber with minimum insertion loss. These three primary considerations make up the discussion of this section.

It is necessary to focus the beam in order to launch it down a fiber optic cable. The beam profile exiting the modulator was measured in the same manner as described previously for the laser beam diameter. It was found that the beam profile spread in width by approximately one half centimeter in passing through the modulator, that is, the diameter of the beam exiting the modulator was experimentally determined to be approximately 1.7 mm (Figure 29).

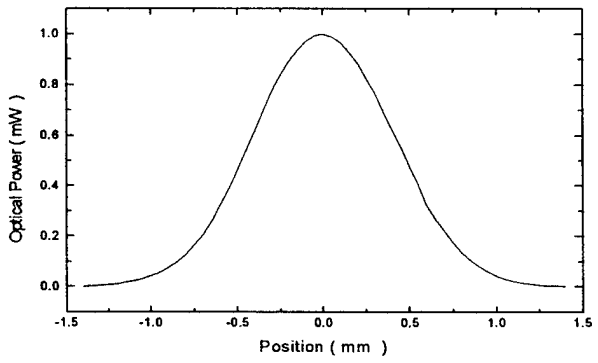

Figure 29. Plot of laser beam power versus transverse position. The beam width is approximately 1.7 mm.

A 500 m communications grade optical fiber with a numerical aperture of 0.29 is used in the experiment. The first step is to determine the lens characteristics necessary to focus the beam. This calculation is dependent on the diameter of the laser beam and the numerical aperture of the fiber optic cable. If n_1 is the index of refraction of the core and n_2 is the index of refraction of the cladding, the numerical aperture is

$$NA = \sqrt{n_1^2 - n_2^2} \quad . \quad (4.1)$$

The numerical aperture is related with the ability of the fiber to guide rays. An optical ray is guided by total internal reflections within the fiber core, provided that the angle of incidence on the core-cladding boundary is greater than the critical angle $\theta c = \sin^{-1}(n_2/n_1)$, measured with respect to the normal at the core-cladding interface (Figure 30). Thus, for a ray incident from air into a fiber to become guided, the angle θ it makes with the fiber axis must be smaller than the complementary angle for total internal reflection θc. At the air-core boundary, the angle θ_0 in air corresponding to $\pi/2-\theta c$ in the core is given by Snell's Law

$$\sin(\theta_0) = n_1 \sin(\pi/2-\theta c) = n_1 \cos(\theta c) \, , \qquad (4.2)$$

By using the value for θc, we find

$$\sin(\theta_0) = n_1 \left[1 - \left(\frac{n_2}{n_1} \right)^2 \right]^{\frac{1}{2}} = \sqrt{n_1^2 - n_2^2} \quad . \qquad (4.3)$$

Therefore,

$$\theta_0 = \sin^{-1}(NA) \quad . \qquad (4.4)$$

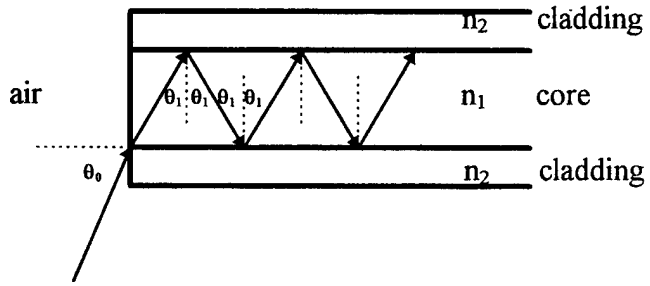

Figure 30. Light ray diagram for a step-index fiber optic cable.

Equation (4.4) defines a cone of angles that the fiber can accept for propagation. Thus, a focused beam within the cone determined by θ_0 will be guided (Figure 31).

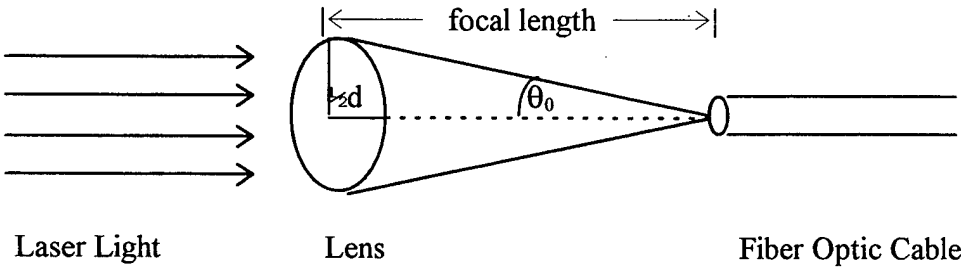

Figure 31. Focusing a collimated light source into a fiber optic cable.

From the trigonometry of the above drawing $\tan(\theta_0) = (\frac{1}{2}d) / f$, where d is the diameter of the laser beam and f is the focal length of the lens. Thus, the focal length of the lens necessary to launch the laser light down the fiber optic cable is

$$f \geq \frac{d}{2\tan\left[\sin^{-1}(NA)\right]} \quad . \qquad (4.5)$$

For a numerical aperture of 0.29 and a laser beam diameter of 1.7 mm, equation (4.5) yields a focal length of approximately 2.8 mm. A focal length slightly higher than this should be used to allow for losses at bends in the optical fiber.

Typical microscope objective lenses are labeled with two numbers corresponding to magnifications and numerical apertures. The overall magnification of a microscope is the product of the linear magnification of the objective multiplied by the angular magnification of the eyepiece when viewing the final image at infinity [5]. It is difficult to determine the exact focal length of most microscope objective lenses with only the information stamped on them.

Table 1 shows approximate values of focal lengths for several common microscope objectives. These values should be treated only as a general guide since precise values vary slightly from lens to lens and manufacturer to manufacturer.

4x	42.50 mm
10x	17.00 mm
20x	8.50 mm
40x	4.25 mm
60x	2.80 mm
100x	1.70 mm

Table 1. Approximate values of focal lengths for several common microscope objectives.

Without a well prepared end it will be impossible to get a good launch down a fiber. The cleaved end must be examined under a microscope to be sure the face is flat, perpendicular to the fiber, and that there are no cracks in the glass. The best way to obtain a good cleave is with a sharp razor blade or specialized tool designed for this purpose. A small score is made in the fiber and tension is then applied from both ends to break the

glass with a clean surface. The process requires applying the slightest pressure to score the fiber while simultaneously pulling on the fiber with the other hand. Figure 32 shows what a typical cleaved end will look like under a microscope.

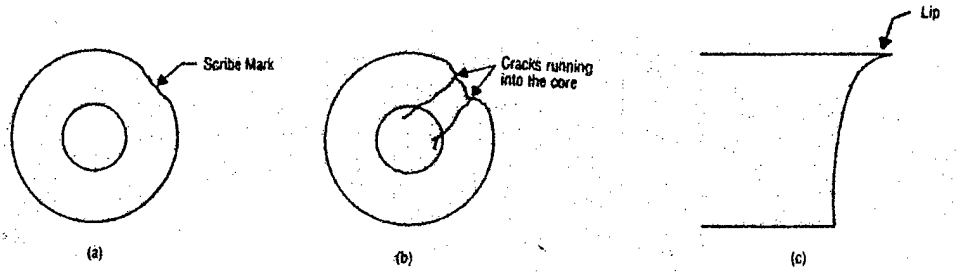

Figure 32. Cleaved fiber ends. (a) Good cleave. (b) Cracked fiber. (c) Side view of a lip. [6]

Once a lens is selected and in position, and the end of the optical fiber is prepared, the final step is to position the end of the fiber at the focal point of the lens. Newport makes a fiber positioner that is designed for this purpose. The end of the fiber optic cable slides into a slotted metal cylinder and a metal filler slides in behind the fiber to hold it in place. The cylinder then slides into a mounting that allows for 3-axis movement. The directions of movement are parallel to the beam, perpendicular to both the beam and the table, and perpendicular to the beam but parallel to the table.

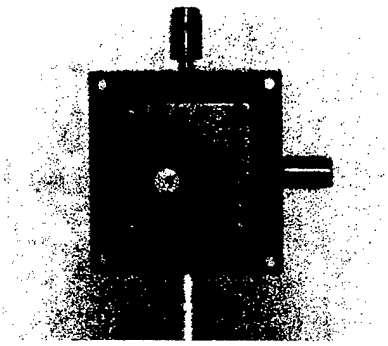

Figure 33. Fiber Optic Positioner with Cylinder to Hold Fiber in Place.

One of these positioners mounts to the back end of the fiber optic coupler. The positioner allows for extremely fine adjustments in the three different directions and in this way the fiber can be positioned precisely for propagation of the light down the cable.

B. ATTENUATION

If a beam of power P_i is launched into one end of a fiber optic cable, and if P_f is the power remaining after a length L (in kilometers) has been traveled, then the attenuation in db/km is given by

$$\text{Attenuation} = \frac{10\log\left(\frac{Pi}{Pf}\right)}{L} \quad . \qquad (4.6)$$

Optical transmission loss (attenuation) in fibers is wavelength-dependent. The two primary loss mechanisms intrinsic to fibers are absorption bands of the material and scattering from inhomogeneities in the refractive index of the fiber. The inhomogeneities are due to thermal fluctuations when the fiber is in the molten state and to impurities in the glass. As the fiber solidifies, these fluctuations cause variations in the index of refraction. If the scale of these variations is of the order of $\lambda/10$ or less, each irregularity acts as a point source Rayleigh scattering center [7]. Absorption losses are mainly from the presence of impurities in the fiber material. A graph depicting the attenuation versus wavelength from 0.7 μm to 1.6 μm of a typical silica-based optical fiber is shown below in Figure 34.

Most of the success in reducing attenuation has come from better control of impurity concentrations. The only real impurity of consequence that remains in optical fibers of today is water in the form of (OH^-) radicals. The absorption bands for (OH^-) are at 950, 1250, and 1380 nm [7]. Outside of these absorption bands, Rayleigh scattering

is the dominant loss mechanism. Quality fibers are sometimes characterized by how closely they approach the Rayleigh scattering limit [6]. An extrapolation of the Rayleigh scattering from Figure 34 to lower wavelengths is shown in Figure 35.

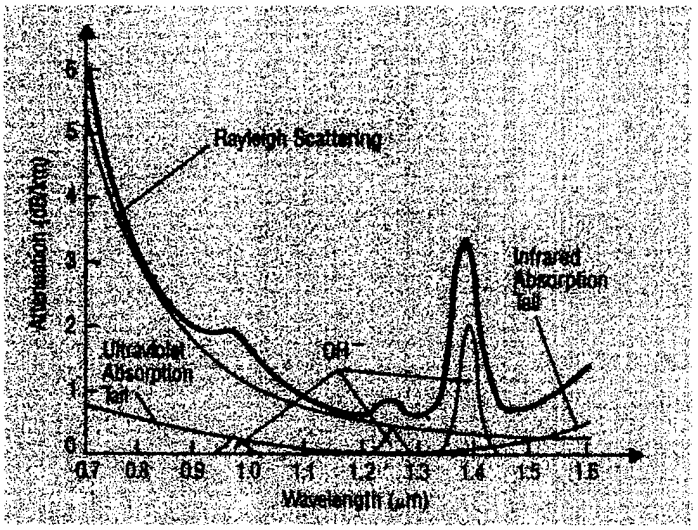

Figure 34. Attenuation of an optical fiber as a function of wavelength [6].

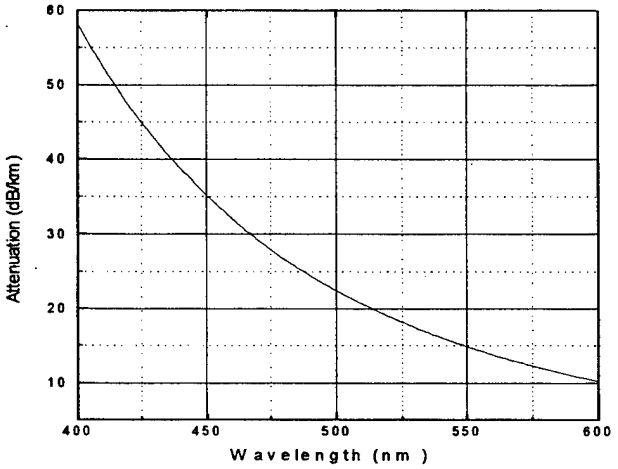

Figure 35. Extrapolated Rayleigh scattering curve.

Attenuation for the 500 m of optical fiber was measured to be approximately 23 $dBkm^{-1}$ with a P_i of 30 mW and a P_f of 2.8 mW. An objective lens of 40 times with a focal length of 4.3 mm was used to focus the laser beam. The experimental value of 23 $dbkm^{-1}$ is near the Rayleigh limit of approximately 20 $dBkm^{-1}$ which can be deduced from Figure 35 for a wavelength of 514.5 nm.

V. CONCLUSIONS AND RECOMMENDATIONS

The primary objectives of this thesis research were outlined at the end of Chapter I. The results of the research are briefly summarized here.

Attenuation of green light, such as the 514.5 nm argon ion laser output, in a silica-based optical fiber is approximately 20 dB/km due to Rayleigh scattering. This means that the optical power output of the laser must be increased in order to have an appreciable amount of light at the end of a long length of fiber. Because of this requirement, experiments with the modulator were conducted with a significant amount of optical power, on the order of 60 mW. The modulator did not perform as well as specified by the manufacturer when confronted with this load of optical power. Further tests are required to determine if the behavior of the modulator is primarily a result of high optical power input, an electrical or electro-optical problem, or some other effect.

Once it is warm, the laser produces a very stable spectral output. However, it does not produce a single mode, monochromatic spectral line. When the laser is directed through the modulator, the structure on the laser profile tends to blur. That is, the valleys in the spectral profile become filled, indicating that additional spectral structure is being injected by the modulator. This effect increases when DC bias voltage is applied to the modulator. Additionally, when the modulator is driven with an AC modulation superimposed on the DC bias voltage, the resultant optical spectral profile does not correspond to that expected for sinusoidal amplitude modulation. It appears that some nonlinear behavior is taking place as the beam passes through the modulator. It has been speculated [8] that this unexpected behavior may be due to Brillouin scattering [9] of

photons by thermal phonons in the KDP modulator crystals. This would account for the blurring of spectral detail. However, verification or refutation of this hypothesis will require additional work.

It is recommended that follow-on work begin at the beginning with DC characterization curves of the modulator. It must be determined whether the modulator is to be aligned as if it were a quarter waveplate, a whole waveplate, or some other configuration with no DC voltage applied. Then DC curves such as the one presented in Figure 9 should be constructed at various levels of optical power input to the modulator from the laser. From there, experiments can be designed to attempt and understand more about the issues of the modulator discussed above and throughout this paper. A good place to start may be to cool the modulator and study the effects of temperature on its behavior.

LIST OF REFERENCES

1. Larraza and Coleman, *Nonlinear Propagation in Optical Fibers: Applications to Tunable Lasers*, Andres Larraza, paper prepared for thesis students.

2. *Model 85 Ion Laser Operator Manual*, Cooper LaserSonics Inc., 1984.

3. Michael C. Ladner, *Optical Modulator LM0202P Characteristics*, Naval Postgraduate School Thesis, June 1996.

4. Sybil P. Parker, *Encyclopedia of Physics*, McGraw-Hill, 1982.

5. Frank L. Pedrotti and Leno S. Pedrotti, *Introduction to Optics*, Prentice-Hall, Inc., 1987.

6. *Projects in Fiber Optics*, Newport Corporation, Fountain Valley, CA.

7. J. Wilson and J.F.B Hawkes,*Optoelectronics, An Introduction, Second Edition*, Prentice Hall, Englewood Cliffs, New Jersey, 07632,1989.

8. D. Scott Davis, Professor of Physics Naval Postgraduate School, Personal Conversation.

9. Bendow, Birman and Agranovich, *Theory of Light Scattering in Condensed Matter*, Plenum Press, 1976.

INITIAL DISTRIBUTION LIST

1. Defense Technical Information Center.....2
   8725 John J. Kingman Rd., STE 0944
   Ft. Belvoir, Virginia 22060-6218

2. Dudley Knox Library.....2
   Naval Postgraduate School
   411 Dyer Rd.
   Monterey, California 93943-5101

3. Dr. W. B. Colson, Code PH/Co.....1
   Department of Physics
   Naval Postgraduate School
   Monterey, California 93943-5002

4. Professor A. Larraza, Code PH/La.....2
   Department of Physics
   Naval Postgraduate School
   Monterey, California 93943-5002

5. Professor S. Gnanalingham, Code PH/Gm.....1
   Department of Physics
   Naval Postgraduate School
   Monterey, California 93943-5002

6. Professor Scott Davis, Code PH/Dv.....1
   Department of Physics
   Naval Postgraduate School
   Monterey, California 93943-5002

7. Professor J. H. Luscombe, Code PH/Lj.....1
   Department of Physics
   Naval Postgraduate School
   Monterey, California 93943-5002

8. Professor D. Walters, Code PH/We.....1
   Department of Physics
   Naval Postgraduate School
   Monterey, California 93943-5002

9. Commandant (G-SIR).....2
   2100 Second Street S.W.
   Washington, DC 20593-0001

10. Commandant (G-SEC)..... 1
2100 Second Street S.W.
Washington, DC 20593-0001

11. Commanding Officer..... 2
USCG R&D Center
1082 Sheene Cossette Road
Groton, CT 06340-6096

12. LT Michael C. Ladner..... 2
2350 South 2300 East
Salt Lake City, UT 84109

13. LT Harlan V. Wallace..... 2
4479 Camille St
Salt Lake City, UT 84124